

How cores grow by pebble accretion

M. G. Brouwers, A. Vazan, and C. W. Ormel

Anton Pannekoek Institute, University of Amsterdam, Science Park 904, PO box 94249, Amsterdam, The Netherlands
e-mail: mgbrouwers@gmail.com; A.Vazan@uva.nl; c.w.ormel@uva.nl

August 21, 2017

ABSTRACT

Context. Planet formation by pebble accretion is an alternative to classical core accretion. In this scenario, planets grow by the accretion of cm-to-m-sized pebbles instead of km-sized planetesimals. One of the main differences with classical core accretion is the increased thermal ablation rate experienced by pebbles. This provides early enrichment to the planet's envelope, which influences its subsequent evolution and changes the process of core growth.

Aims. To describe and compute core growth in the pebble accretion model. We aim to predict core masses and compositions that can form by pebble accretion and compare them to the case of planetesimals.

Methods. We have written a code containing both an impact and a planet evolution model to simulate the early growth of a proto-planet self-consistently. The region where high-Z material (in our case SiO_2) can exist in vapor form is determined by the temperature-dependent vapor pressure. We include enrichment effects by locally modifying the mean molecular weight of the envelope and determine when direct core growth of the planet terminates.

Results. We have identified three phases of core growth in pebble accretion. In the first phase ($M_{\text{core}} < 0.23\text{--}0.39 M_{\oplus}$), pebbles impact the core without significant ablation. During the second phase ($M_{\text{core}} < 0.5 M_{\oplus}$), ablation becomes increasingly severe. A layer of high-Z vapor starts to form around the core that absorbs a small fraction of the ablated mass. The rest of the material either rains out to the core or mixes outwards instead, slowing core growth. In the third phase ($M_{\text{core}} > 0.5 M_{\oplus}$), the high-Z inner region expands outwards, absorbing an increasing fraction of the ablated material as vapor. Rainout ends before the core mass reaches $0.6 M_{\oplus}$, terminating direct core growth.

Conclusions. Our results indicate that pebble accretion can directly form rocky cores up to only $0.6 M_{\oplus}$, and is unable to form icy cores. This result contrasts classical core accretion models, which can directly form massive cores of both rocky and icy compositions. Subsequent core growth can proceed indirectly when the planet cools, provided it is able to retain its high-Z material.

Key words. Methods: numerical – Planetary systems – Planets and satellites: composition – Planets and satellites: formation – Planets and satellites: physical evolution – Planet-disk interactions

1. Introduction

The growth of planetary cores is a conceptually simple process in the classical core accretion scenario. An increasingly massive planetary embryo is impacted by large, km-sized impactors that add to its mass (Pollack et al. 1996; Hubickyj et al. 2005). Soon, the small proto-planet starts to gravitationally bind an envelope of gas. This envelope is initially very poor in high-Z material due to the limited interaction between the envelope and any impacting planetesimals (Podolak et al. 1988). Core growth eventually comes to a halt when the planet has no more solid material left in its feeding zone to accrete. Unfortunately, the classical core accretion scenario faces a time-constraint problem. Simulations indicate that this way of planet formation typically requires more time than the expected lifetimes of the disks from which their matter originates (Kobayashi et al. 2010; Levison et al. 2010; Bitsch et al. 2015). While i.e. Alibert et al. (2005) have shown that including effects as migration and disk evolution can reduce formation times in some cases, another option is to look at new formation models which do not face the same problem

One such scenario is *pebble accretion* (Ormel & Klahr 2010; Lambrechts & Johansen 2012). Instead of km-sized planetesimals, the proto-planet accretes smaller, cm-m-sized objects, called *pebbles*. There are two main differences that originate from this size difference. Firstly, pebble accretion is expected to have an accretion rate of approximately an order of magnitude

above typical rates for planetesimals (Lambrechts et al. 2014), and operates particularly well when the pebbles are settled into the mid-plane regions (Ormel 2017). The reason for this is the more efficient capturing of pebbles due to their increased susceptibility to gas drag. Secondly, pebbles have more interaction with a planet's atmosphere. Their larger area-to-mass ratio makes it easier for them to be slowed down by aerodynamic gas drag and reduces their ablation timescales (e.g. Love & Brownlee 1991; McAuliffe & Christou 2006). As a result, these pebbles can deposit high-Z vapor into even a small growing planet. This in turn can have a large effect on the planet's further growth and evolution (Venturini et al. 2016). The presence of high-Z material locally increases the mean molecular weight, which drives up densities and temperatures, increasing the envelope mass.

So far, research on pebble accretion has mainly focused on the first difference by calculating accretion rates though disk evolution and drag considerations (e.g. Morbidelli & Nesvorný 2012; Chambers 2014; Ida et al. 2016). The evaporation effects have only recently been considered by Alibert (2017), based on impact simulations by Benz et al. (2006). He estimated the maximum core masses for which 0.1 m pebbles are expected to be able to reach the core. In his simulations, direct core impacts terminate when the planet becomes either too hot ($T_{\text{core}} > 1600$ K) or the envelope becomes too massive ($M_{\text{env}} > 10^{-4} M_{\oplus}$) for pebbles to reach the core. He found these conditions to be met before

the core grew to $1 M_{\oplus}$. However, he neglected any enrichment up to the point that pebbles are expected to be fully evaporated and did not compute the evolution beyond this ablation point. In reality, the core can continue to grow if the ablated material over-saturates the gaseous atmosphere, and leftover material rains out to the core (Iaroslavitz & Podolak 2007).

In this work, we investigate how cores grow by pebble accretion. We expand previous calculations of core growth by including enrichment effects from when they first occur and by considering further growth through the rainout of ablated material. Our code simulates planet formation along with pebble impacts in a way that quantitatively incorporates the pebble's interaction with the growing atmosphere. We calculate the effects of ablation and gas drag on impacting pebbles and relate these effects to the planet's subsequent evolution by modifying the luminosity profile and mass deposition curve. Core growth itself also depends on whether solid high-Z material can make it to the core surface. Our results show that impacting pebbles may be fully ablated before the planet even reaches $0.5 M_{\oplus}$. Subsequent rainout of ablated material can add some additional mass, but it seems hard to form M_{\oplus} -sized cores directly by pebble accretion.

This paper is organized as follows. Sections 2.1 and 2.2 introduce our impact and planet simulation models. Section 2.3 elaborates on our treatment of high-Z enrichment and the rainout of ablated material to the core. Our results are presented in Sect. 3 and compared to the case of classical core accretion in Sect. 4. Section 5 covers the discussion and conclusions.

2. Model description

The goal of this work is to provide an estimate of the core sizes that planets can form directly by pebble accretion. To that effect, we focus on the first stage of planet formation when the planet's accretion is still dominated by solids instead of disk gas. In this scenario, a growing proto-planet is constantly being impacted by small, cm-m-sized objects. These impactors partially or fully evaporate during entry and contribute high-Z material (in our case SiO_2 , quartz) to the core and envelope. To simulate the planet's growth, we used a new evolution code consisting of two components. The first is a time-dependent calculation of the planet's structure and gas accretion rate. We model its evolution as is typically done by a series of quasi-hydrostatic models with a separate core and envelope (e.g. Mordasini et al. 2012; Piso & Youdin 2014). The second component is a calculation of the interaction between impacting pebbles and the planet's atmosphere. The accretion of solids is modeled by a single-body simulation code that uses the layers generated by the structure code. Impactors hit the planet head-on and lose mass by thermal ablation and friction. The resultant core accretion and mass deposition rates affect the planet's further evolution. In principle, the two codes should be iterated to make sure they work self-consistently. In tests, one iteration was found to be sufficient to achieve this. Therefore we run them twice during every timestep.

2.1. Impact model

Gas drag

Impacting pebbles are modeled as perfect spheres with a uniform size and a constant density of $2.65 \times 10^3 \text{ kg m}^{-3}$. For simplification, these impactors are assumed to hit the planet head on. In this sense, we study the limit where pebbles can most easily reach the core. Their initial velocities are equal to the lower of

the terminal and escape velocities. The first is a drag-induced limitation, calculated by the velocity at which the local drag force is exactly equal in magnitude to the gravitational force. The second is the limitation of the total gravitational energy that an impactor can acquire as it moves towards the planet. As impactors approach the core, gravity accelerates them and gas drag slows them down. The drag force is given by

$$F_{\text{drag}} = 0.5 C_d A \rho_g v^2 \quad (1)$$

where ρ_g the gas density, A the impactor's frontal area, v its relative velocity to the gas and C_d the drag constant. Most of the physics is contained in this drag constant. For our purposes, we want to be able to describe drag over a wide range of conditions, for impactors varying in size from 1 cm up to several kilometers. There has been extensive research on empirical expressions for different drag regimes. We adopt an extended version of the widely applicable expression by Melosh & Goldin (2008), based on a review of this literature. Theirs is a continuous expression of C_d that is applicable to a large range of conditions. It depends on the local mach number $\text{Ma} = v/c_s$, the Reynolds number $\text{Re} = vR/\eta_g$ where η_g is the dynamical viscosity of the gas and R is the impactor radius, and on Knudsen's number (Kn) which is defined as the ratio between the Mach and Reynolds numbers, $\text{Kn} = \frac{\text{Ma}}{\text{Re}}$. The full expression for C_d reads:

$$C_d = 2 + (C_1 - 2) \exp[-3.07 \sqrt{\gamma_g} \text{Kn} C_2] + H \frac{1}{\sqrt{\gamma_g} \text{Ma}} e^{-1/2 \text{Kn}} \quad (2)$$

where C_1 , C_2 and H are the auxiliary functions

$$C_1 = \frac{24}{\text{Re}} \left(1 + 0.15 \text{Re}^{0.678} \right) + \frac{0.407 \text{Re}}{\text{Re} + 8710} \quad (3)$$

$$\log C_2 = \frac{2.5 (\text{Re}/312)^{0.6688}}{1 + (\text{Re}/312)^{0.6688}} \quad (4)$$

$$H = \frac{4.6}{1 + \text{Ma}} + 1.7 \sqrt{\frac{T_p}{T_g}} \quad (5)$$

and T_p and T_g are the impactor's surface temperature and the local gas temperature respectively. γ_g is the adiabatic index of the gas, explained in detail in Sect. 2.2. C_1 is an extended version of the expression given by Melosh & Goldin (2008) as suggested by D'Angelo & Podolak (2015), based on an empirical review from Brown & Lawler (2003). Their expression only breaks down at Reynolds numbers exceeding approximately 3×10^5 , when the type of flow around the sphere becomes turbulent. We have modeled this turbulent part of the flow by a step-function decrease of C_d to 0.2 (e.g. Michaelides 2006). To illustrate the importance of including a varying drag constant, Fig. 1 shows the drag constant evolution of a 0.1 m SiO_2 pebble impacting a $0.3 M_{\oplus}$ planet at escape velocity. During this impact, Kn is near unity at the edge of the planet and drops close to zero as the pebble approaches the core. In this regime, $\text{Kn} < 1$ and $\text{Ma} > 1$ for most of the impact, resulting in values of C_d that are considerably different from the low- v drag expressions typically used in the planet formation literature (Weidenschilling 1977; Whipple 1972).

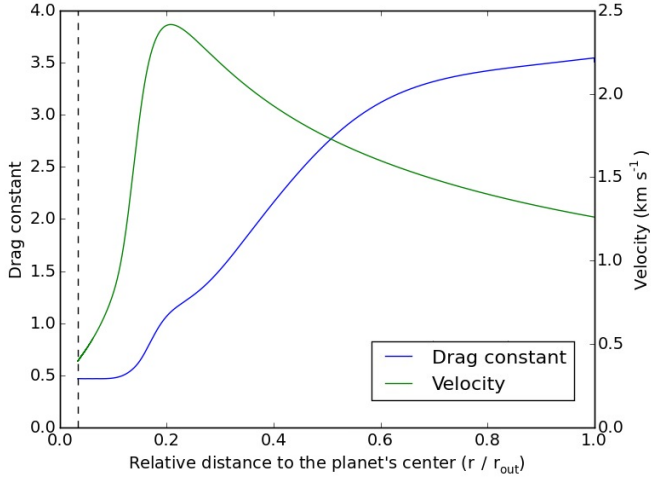


Fig. 1. The drag constant evolution of a 0.1 m SiO₂ pebble impacting a 0.3 M_⊕ planet at escape velocity. The blue line represents the drag constant, the green line is the impactor's velocity relative to the surrounding gas and the black dashed curve represents the core radius.

Ablation

When an impactor enters the planet's envelope, it becomes surrounded by increasingly hot gas. We include two heating mechanisms; radiation and friction. Thermal radiation is approximated by perfect Planck curves. The net total of irradiated energy is then given by the Stefan-Boltzmann expression with the area of a sphere:

$$P_{\text{rad}} = 4\pi R^2 \alpha \sigma_{\text{sb}} (T_{\text{g}}^4 - T_{\text{s}}^4) \quad (6)$$

where T_{s} is the pebble's surface temperature and α is its average absorption constant, assumed to be unity. We use ambient gas temperatures even when incoming objects are supersonic. Gas temperatures and densities are highest near the core. We find that thermal ablation in combination with impactors being slowed down typically leads to very localized ablation in this inner region.

For large or fast impactors, frictional heating becomes important. These objects lose significant amounts of kinetic energy, a fraction f_{h} of which gets converted into heat.

$$P_{\text{fric}} = f_{\text{h}} F_{\text{drag}} v \quad (7)$$

Estimating the numerical value of f_{h} is a complex problem. Most works on impacts assume it to be equal to some constant of varying size (e.g. Podolak et al. 1988; Pinhas et al. 2016). We allow f_{h} to vary during the impacts and evaluate f_{h} based on gas characteristics, with the expressions from Melosh & Goldin (2008):

$$f_{\text{h}} = \frac{8}{\gamma_{\text{g}}} \left(\frac{\text{Nu}}{\text{RePr}} \right) \frac{r'}{C_{\text{d}}} \quad (8)$$

where r' is the recovery factor, evaluated as $r' = (\text{Pr})^{\frac{1}{3}}$ (Mills 1999). In addition to Re, f_{h} further depends on the Nusselt (Nu) and Prandtl (Pr) numbers

$$\text{Nu} = \frac{Nu_{\text{c}}}{1 + 3.42M'Nu_{\text{c}}/\text{RePr}} \quad (9)$$

$$\text{Pr} = \frac{\eta_{\text{g}} C_{\text{p,g}}}{k_{\text{g}}} \quad (10)$$

where $C_{\text{p,g}}$ is the specific heat of the gas, Nu_{c} and M' are auxiliary functions

$$Nu_{\text{c}} = 2 + 0.459\text{Re}^{0.55} r' \quad (11)$$

$$M' = \frac{\text{Ma}}{1 + 0.428\text{Ma}(\gamma_{\text{g}} + 1)/\gamma_{\text{g}}} \quad (12)$$

and η_{g} is the dynamic viscosity of the gas, the components k of which we evaluate with the common expression from kinematic theory (e.g. Dean 1985)

$$\eta_{\text{k}} = \frac{5}{16d_{\text{k}}^2} \sqrt{\frac{m_{\text{k}} k_{\text{b}} T_{\text{g}}}{\pi}} \quad (13)$$

where d_{k} and m_{k} are the molecular diameter and weight of the gas constituent and k_{b} is the Boltzmann constant. The values of η_{k} are summed by volume fraction to yield η_{g} . In the simulated impacts of pebbles, the friction factor is found to vary between approximately 0.5 and 0.05.

As an impactor heats up, its inner region is initially shielded from the heat. This leads to the formation of a temperature gradient. The importance of this gradient can be inferred from the Biot number:

$$\text{Bi} = \frac{h'L}{k} \quad (14)$$

where h' is the characteristic heat transfer coefficient, L is a characteristic length, equal to $\frac{R}{3}$ for a sphere and k is the thermal conductivity, which we take equal to 2 W K m⁻¹. This is a commonly taken average based on data from Powell et al. (1966) (e.g. Adolfsson et al. 1996). In the context of planetary entry, h' can be approximated as (Love & Brownlee 1991)

$$h' = \sigma_{\text{sb}} \Delta T^3 \quad (15)$$

where ΔT is the temperature difference between the local gas and the impactor's surface. Whenever the Biot number is less than 0.1, an object can roughly be considered as isothermal. A typical first order approach to modeling a temperature gradient is setting the Biot number equal to 0.1 and interpreting the resultant radius as an isothermal layer of temperature T_{s} with depth and mass (e.g. Love & Brownlee 1991; McAuliffe & Christou 2006)

$$d_{\text{iso}} = \min \left(0.3 \frac{k}{\sigma_{\text{sb}} \Delta T^3}, R \right) \quad (16)$$

$$M_{\text{iso}} = \frac{4}{3} \pi r^3 \rho (R^3 - (R - d_{\text{iso}})^3) \quad (17)$$

The total heat contents of the impactor are therefore approximated by $C_{\text{p}} (T_{\text{s}} M_{\text{iso}} + T_{\text{disk}} (M - M_{\text{iso}}))$ where the temperature of the interior region is assumed to be equal to that of the disk, T_{disk} . When the temperature of the surface layer has increased sufficiently, atoms start to evaporate into the envelope. This process can be characterized by the Langmuir formula

$$\dot{m} = 4\pi R^2 P_{\text{v}} \sqrt{\frac{m_{\text{g}}}{2\pi k_{\text{b}} T_{\text{s}}}} \quad (18)$$

where m_{g} is the mean molecular weight of the gas and P_{v} is the vapor pressure of the impactor (see Sect. 2.3). Evaporation prevents the impactor from heating indefinitely. The surface temperature starts to decrease again when the energy loss through

evaporation exceeds the incoming heat. Using the conservation of energy, the impactor's surface temperature can be obtained from

$$4\pi R^2 \alpha \sigma_{\text{sb}} (T_{\text{g}}^4 - T_{\text{s}}^4) + f_{\text{h}} F_{\text{drag}} v - 4\pi R^2 P_{\text{v}} \sqrt{\frac{m_{\text{g}}}{2\pi k_{\text{b}} T_{\text{s}}}} E_{\text{vap}} = C_{\text{p}} (M_{\text{iso}} \dot{T}_{\text{s}} + \dot{M}_{\text{iso}} (T_{\text{s}} - T_{\text{disk}})) \quad (19)$$

where T_{disk} is the local disk temperature, E_{vap} the latent heat upon evaporation, taken to be equal to $8.08 \times 10^6 \text{ J kg}^{-3}$ for SiO_2 as in D'Angelo & Podolak (2015) and C_{p} is the specific heat of the impactor. This is a temperature-dependent parameter that we evaluated with a fit reported on the Chemistry Webbook of the National Institute of Standards and Technology (NIST), based on original measurements by Chase (1998).

In summary, the terms in Eq. (19) denote contributions from respectively radiative cooling, frictional heating, evaporative cooling and internal energy. This temperature balance is invoked to yield the equilibrium temperature of the isothermal layer T_{s} with a resolution of 10^{-3} K at any timestep. Such a precise temperature determination is necessary to ensure numerical stability because of the large temperature dependence of the vapor pressure.

2.2. Planetary structure

We integrate the planet's atmosphere from the outside in, starting at the lower of either the Hill or Bondi radius. At this radius the envelope's composition and conditions are taken to be the same as the disk's. Our code solves for two boundary conditions at the core surface: the mass condition $M(r = r_{\text{core}}) = M_{\text{core}}$ and the luminosity condition

$$L_{\text{core}} = \chi_{\text{core}} \frac{\dot{M}_{\text{acc}} v_{\text{core}}^2}{2} \quad (20)$$

where χ_{core} and v_{core} are the surviving mass fraction and velocity of impactors that reach the core and \dot{M}_{acc} is the solids accretion rate. We consider accretion to be the only energy source at the core and neglect any additional contributions, such as radioactive heating or core contraction. The total luminosity and envelope mass are adjusted such that these conditions are matched at every time-step. Disk gas flows into the envelope to fit the increased interior mass.

The structure of the planet is strictly divided into two parts: a solid core and a gaseous envelope. We use a typical constant density for the core of $3.2 \times 10^3 \text{ kg m}^{-3}$ (e.g. Pollack et al. 1996; Hubickyj et al. 2005). The core grows only when solid material reaches its boundary. In our model, this can occur in two ways. Either by direct impacts of accreting material, or by the rainout of ablated silicates when the vapor saturation of the envelope is exceeded. The envelope's structure is calculated with the one-dimensional spherically symmetric stellar structure equations:

$$\frac{dP}{dr} = \frac{-GM\rho}{r^2} \quad (21)$$

$$\frac{dM}{dr} = 4\pi r^2 \rho \quad (22)$$

$$\frac{dT}{dr} = \frac{dP}{dr} \frac{T}{P} \nabla_{\text{th}} \quad (23)$$

where G is the gravitational constant, P is pressure, T the temperature, M the total mass interior to radius r , ρ the envelope density and r the distance to the planet's center. We use the Schwarzschild criterion to determine the thermal gradient ∇_{th} as $\nabla_{\text{th}} = \min(\nabla_{\text{conv}}, \nabla_{\text{rad}})$ where ∇_{conv} is approximated by the adiabatic gradient ∇_{ad} , which we take as a constant based on the local gas composition

$$\nabla_{\text{ad}} = \frac{\gamma_{\text{g}} - 1}{\gamma_{\text{g}}} \quad (24)$$

where γ_{g} is the average adiabatic index of the gas, defined as the ratio of the specific heat under constant pressure and volume $C_{p_{\text{g}}}/C_{v_{\text{g}}}$. We use data from Chase (1998) to evaluate the compositional components of γ_{g} as a function of temperature. To calculate $C_{v_{\text{g}}}$, we assume constant γ values equal to $\gamma_{\text{H}_2} = 1.4$, $\gamma_{\text{He}} = \frac{5}{3}$ and $\gamma_{\text{SiO}_2} = 1.2$. For the radiative outer zone of the envelope, we use

$$\nabla_{\text{rad}} = \frac{3\kappa LP}{64\pi\sigma_{\text{sb}} GMT^4} \quad (25)$$

where κ is the opacity and L the luminosity. The opacity is assumed to originate only from the gas and is approximated by the analytical expression from (Bell & Lin 1994)

$$\kappa = 10^{-9} \rho^{\frac{2}{3}} T^3 \quad (26)$$

which is valid for molecules. We do not assume a grain opacity, as these are likely to be very low because of coagulation and sedimentation processes (Movshovitz et al. 2010; Mordasini 2014; Ormel 2014).

The luminosity has four components; kinetic energy deposition by the impactors, (negative) latent heat release upon ablation, high-Z rainout and contraction.

$$\frac{dL}{dr} = \left(\frac{dK_{\text{i}}}{dr} - E_{\text{vap}} \frac{d\chi_{\text{i}}}{dr} \right) \dot{M}_{\text{acc}} + \frac{GM\dot{M}_{\text{rain}}}{r^2} - 4\pi r^2 \rho P \dot{V} \quad (27)$$

where K_{i} is the kinetic energy of an impactor, \dot{M}_{rain} is the local rainout rate and V is the specific gas volume $\frac{1}{\rho}$. The core luminosity is determined by the mass fraction (χ_{core}) of the pebbles that reaches the core and their kinetic energy (See Eq. (20)). The structure equations are supplemented by the ideal gas equation of state for a mixed composition

$$\rho = \frac{Pm_{\text{g}}}{k_{\text{b}}T} \quad (28)$$

The range of conditions we experience in our simulations is still well approximated by the ideal gas equation (see Sect. 3.2). Temperatures inside the planet's inner region can exceed those required for the dissociation of hydrogen, but these regions are modeled as silicate-dominated and contain little hydrogen. The effective difference with using a more sophisticated equation of state is therefore minor. An explicit test of this is included in Sect. 3.2.

The structure equations are integrated using a fourth-order Runge-Kutta scheme. We have set the time-step $\Delta t = \Delta M/\dot{M}_{\text{acc}}$ such that the planet accretes $0.005 M_{\oplus}$ at every interval. The grid consists of set logarithmic distances to provide enough resolution near the core and consists of approximately 50,000 layers per integration. The reason for this high number is to ensure a smooth temperature profile of the inner region of the planet. This reduces the number of iterations needed in the impact code and speeds up the run-times.

2.3. High-Z enrichment and rainout

We consider the planet to be embedded in a gaseous disk with mass fractions of 75 % molecular hydrogen and 25 % helium. The initial envelope and the accreted gas do not contain any high-Z materials. However, as the proto-planet is impacted by pebbles, some of their material ablates into the atmosphere before it can impact the core. We consider the effects this has on the planet's further evolution and subsequent impacts by locally increasing the mean molecular weight where high-Z material is present in vapor form. The maximum fraction (by mass) of high-Z vapor that the gas can contain depends on the local silicate vapor- and total pressure:

$$f_{g,\text{SiO}_2,\text{max}} = \frac{\mu_{\text{SiO}_2}}{\mu_g} \frac{P_{\text{vap}}^{\text{SiO}_2}}{P} \quad (29)$$

where f_{g,SiO_2} is the local mass fraction of silicates in vapor phase. Equation (29) can be interpreted as the high-Z saturation curve of the gas, depending on pressure and temperature. Vapor pressures can be expressed by the Clausius-Clapeyron equation

$$P_{\text{vap}}^{\text{SiO}_2} = \exp\left[a_0 - \frac{a_1}{T + a_2}\right] \quad (30)$$

where $a_0 = 29.5$, $a_1 = 46071.4 \text{ K}$, $a_2 = 58.9 \text{ K}$ are constants determined by the fit published on NIST, based on original data from (Stull 1947). We iterate on μ_g at every time-step to ensure an accurate estimation. When the gas temperature becomes such that $f_{g,\text{SiO}_2} > 1$, we limit f_{g,SiO_2} to unity. In this case, the atmospheric layer consists entirely of silicate gas. The temperature dependency of the vapor pressure limits the presence of silicate vapor to the envelope's warmer interior layers. Finding the partial pressure also requires identifying how much total silicate mass is present in a given layer. This is affected by the amount of material that has been ablated up to that point and also depends on what happens to the silicates after ablation (i.e. outward mixing or settling). To simplify matters, we look at two contrasting scenarios:

1. In the *mixing* case, we assume that all the ablated material mixes uniformly through the entire envelope. This includes the material in solids as well as in vapor form. We track the total high-Z mass that has ablated up to that point in time, $M_{Z,\text{abl}}$. During this time, the planet has also attracted hydrogen and helium gas masses M_{H_2} and M_{He} from the disk. Complete mixing then leads to one global silicate mass fraction (vapor + solids) that is calculated as

$$f_{\text{SiO}_2} = \frac{M_{Z,\text{abl}}}{M_{Z,\text{abl}} + M_{\text{H}_2} + M_{\text{He}}} \quad (31)$$

In the outer layers, $f_{\text{SiO}_2} > f_{g,\text{SiO}_2}$ and most of the silicate mass is in solids. This trend continues inward up to the point that the temperature of a layer is sufficiently high that $f_{\text{SiO}_2} = f_{g,\text{SiO}_2}$. Here, mixing limits the silicate vapor mass fraction to f_{SiO_2} of Eq. (31). Direct core growth in this scenario only continues as long as some part of the impactors can directly reach the core.

2. In the *rainout* case, any material in excess of what can be contained in vapor (see Eq. (29)) falls to the layer below. The resulting rainout of high-Z material increases the planet's luminosity as descending silicate mass loses gravitational energy on its way to the core. If the envelope cannot absorb all the ablated material, the rest of it adds to the core mass. This allows the core to grow beyond the point that impactors fail

Table 1. Descriptions and values of the standard model parameters

Parameter	Description	Value
R_{impactor}	Impactor radius	0.1 m
v_{start}	Starting velocity impactor	$\min(v_{\text{terminal}}, v_{\text{esc}})$
$f_{\text{H}_2}, f_{\text{He}}$	Disk mass fractions	0.75, 0.25
T_{disk}	Local disk temperature	150 K
d_{planet}	Orbital radius	5.2 AU
M_{\star}	Mass of the central star	$1 M_{\odot}$
ρ_{disk}	Local disk density	$5 \times 10^{-8} \text{ kg m}^{-3}$
\dot{M}_{acc}	Solids accretion rate	$10^{-5} M_{\oplus} \text{ yr}^{-1}$

to reach the core directly. Direct core growth ceases when all the accreting solids can be fully absorbed by the envelope as vapor.

Vapor pressures rise quickly as the local gas temperature increases. Close to the core, conditions can be such that the vapor pressure exceeds the total pressure and the high-Z mass fraction approaches one. The high mean molecular weight of this high-Z layer surrounding the core leads to very steep pressure and density curves as can be seen in Fig. 4 of the next section.

3. Results

3.1. Standard model

The simulations shown here use the parameters from Table 1 unless specifically stated otherwise. We simulate the planet at a distance of 5.2 AU from the central star, embedded in a disk with a typical local temperature and density of 150 K and $5 \times 10^{-8} \text{ kg m}^{-3}$ (Hubickyj et al. 2005). We use a standard pebble accretion rate of $10^{-5} M_{\oplus} \text{ yr}^{-1}$ (Lambrechts et al. 2014). The goal is to estimate how much a core can grow before direct core accretion stops. This is either when impacting pebbles fully evaporate in our *mixing* scenario, or when the atmosphere can absorb all ablated material in the *rainout* case. Figure 2 shows the result of our simulation for both of these assumptions.

In general, we can distinguish three phases of core growth:

1. When the core mass is still below $\sim 0.23\text{--}0.39 M_{\oplus}$, depending on impactor size, all pebbles can reach the core without experiencing significant thermal ablation.
2. After this point, ablation becomes increasingly severe and a decreasing mass fraction impacts the core directly. The planet's temperature and pressure are still too low for the envelope to be able to retain significant amount of silicate vapor, causing the rest to rain out. If the ablated material mixes outwards instead, core growth slows down.
3. Around $0.50 M_{\oplus}$, the planet's envelope mass and temperature have increased sufficiently for absorption of high-Z vapor in the envelope's inner region to become significant. Impactors can be fully ablated in the atmosphere and direct core impacts terminate. The planet becomes heavily enriched during this third phase, leading to the formation of a high-Z layer around the core with a very high density and temperature.

To further illustrate the core growth process, we have plotted the envelope-to-core ratio of a growing planet along with its absorption rates in Fig. 3. The absorption rate is defined as the fraction of ablated accreting material that stays in the atmosphere in vapor form. The planet's envelope-to-core ratio starts to increase rapidly after its core mass reaches $\sim 0.5 M_{\oplus}$. This coincides with

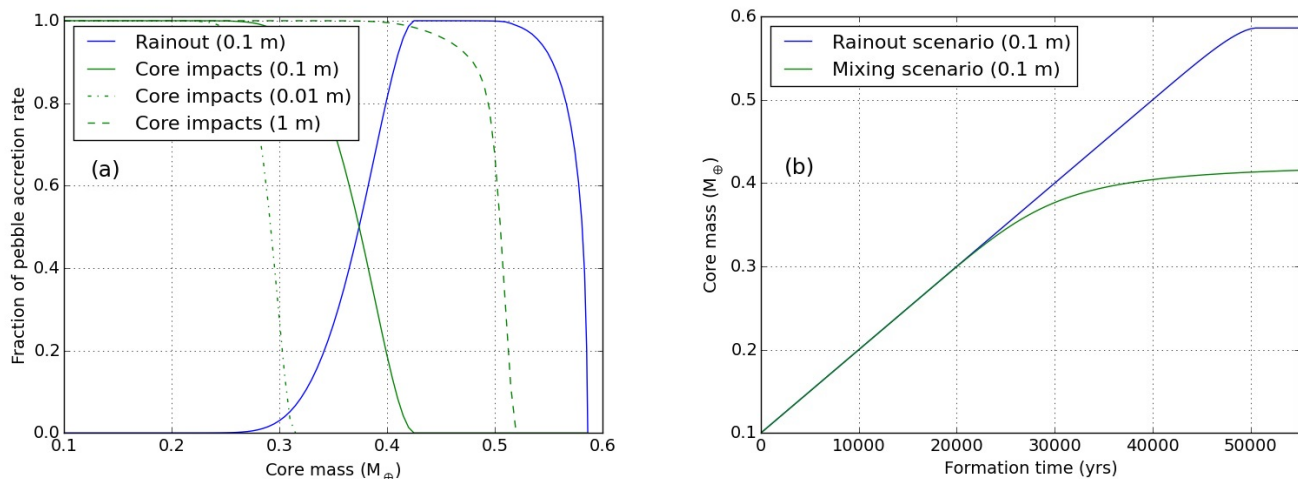


Fig. 2. Core growth by pebble accretion. The left Fig. (a) shows the mass fractions of solids impacting the core directly (green curves), or reaching the core by rainout of ablated material (blue curve). The differently spaced green curves correspond to three sizes of pebbles; 0.1 m (solid), 1 m (dashed), 0.01 m (dash-dot). The right Fig. (b) shows the growth of the core over time. In this figure, the *rainout* scenario is indicated by the blue curve and the *mixing* case is shown by the green curve. Both curves in Fig. (b) correspond to 0.1 m impactors.

the formation of a high-Z layer near the core, as can be seen by the simultaneous increase of the absorption rate. The envelope mass is at first mostly due to hydrogen and helium gasses. When absorption becomes significant, the envelope’s metal rich inner region becomes very hot and dense and its constituting silicate vapor starts to dominate the envelope mass.

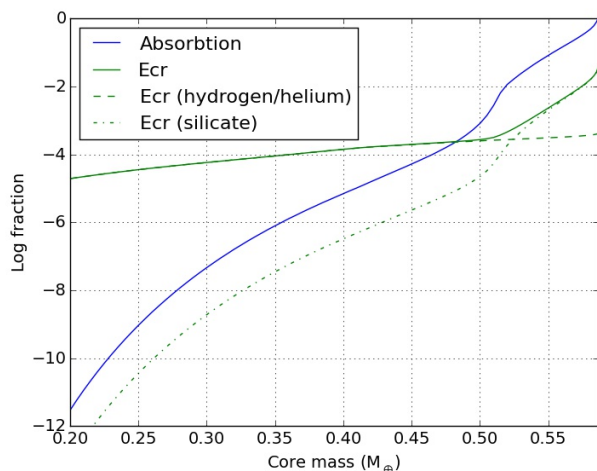


Fig. 3. The absorption fraction (blue) and envelope-to-core ratio (*ecr*; green) of a planet impacted by 0.1 m pebbles. The green curves indicate the envelope-to-core ratio, defined as $M_{\text{env}}/M_{\text{core}}$. The dash-dot curve is its silicate mass fraction and the dashed curve is its hydrogen and helium mass fraction. They sum to the total *ecr*, shown by the solid green line. The blue absorption curve indicates the mass fraction of the accreting solids that can be contained by the envelope as vapor.

The temperature, density, pressure and high-Z enrichment curves of the resulting planet are plotted in Fig. 4. The gas of the enriched inner region has a much higher mean molecular weight in the *rainout* case, causing it to become very hot and dense.

Table 2. The variation of final core masses for different pebble sizes, disk conditions and accretion rates. The final column (left and right) shows the core masses at which either pebbles are fully evaporated (*mixing scenario*; left) or all ablated material can be absorbed by the envelope as vapor (*rainout scenario*; right).

Variation	Value	Final core masses (M_{\oplus})	
–	–	0.42	0.59
R_{impactor}	0.01 m	0.31	0.59
R_{impactor}	1 m	0.52	0.58
EOS	(Vazan et al. 2013)	0.42	0.59
\dot{M}_{acc}	$10^{-4} M_{\oplus} \text{ yr}^{-1}$	0.41	0.55
\dot{M}_{acc}	$10^{-6} M_{\oplus} \text{ yr}^{-1}$	0.42	0.65
d_{planet}	10 AU	0.40	0.60
d_{planet}	1 AU	0.41	0.54
d_{planet}	0.5 AU	0.33	0.48
d_{planet}	0.2 AU	0.23	0.37
μ_{SiO_2}	40 g mol^{-1}	0.42	0.66
μ_{SiO_2}	18 g mol^{-1}	0.43	0.97
μ_{SiO_2}	10 g mol^{-1}	0.44	1.49
γ_{SiO_2}	1.4	0.42	0.66
γ_{SiO_2}	1.1	0.42	0.57

3.2. Model sensitivities and limitations

To check the sensitivity of our results to the variation of several parameters, we have performed the same simulations with different pebble sizes, disk orbital radii, solid accretion rates or SiO_2 characteristics (see Table 2). The disk conditions for different planet positions correspond to an extrapolation of the conditions we chose at 5.2 AU. We used MMSN scaling, so $T_{\text{disk}} \propto r^{-0.5}$ and $\rho_{\text{disk}} \propto r^{-2.75}$ (e.g. Weidenschilling 1977; Hayashi 1981). The last columns of Table 2 show the final core masses for various sets of parameters. These represent the points at which pebbles are either fully evaporated (*mixing*) or all ablated material can be absorbed as vapor (*rainout*).

To zeroth order, the computed final core masses shown in Table 2 can be predicted by the point at which the core surface temperature first exceeds about 1600 K, and SiO_2 starts evaporating. Our general picture of limited core growth does not change

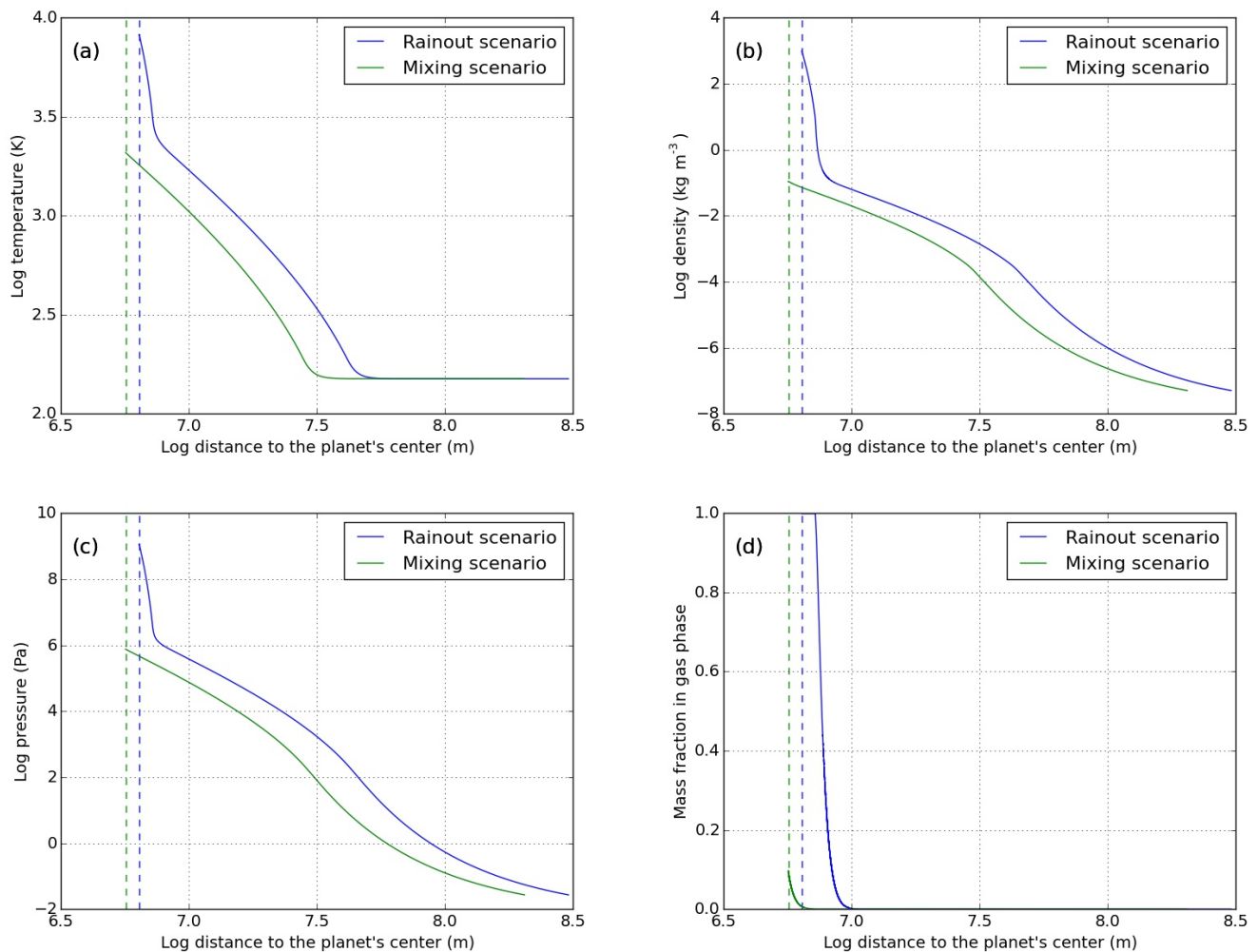


Fig. 4. The temperature (a), density (b), pressure (c) and high-Z enrichment (d) interior curves at the point when core growth is equal to 10 percent of the pebble accretion rate. This corresponds to core masses of $0.58 M_{\oplus}$ in the *rainout* scenario (blue curves) and $0.41 M_{\oplus}$ in the *mixing* case (green curves).

when we vary the pebble size, disk conditions or the solids accretion rate. The inner atmosphere always reaches 1600 K at a core mass of $\sim 0.3 M_{\oplus}$. As expected, smaller pebbles evaporate sooner than larger ones, thus leading to a lower core mass in the *mixing* case. Final core masses after *rainout* terminates, are less significantly influenced by pebble size because the envelope’s absorption rates do not change.

These absorption rates do change when the accretion rate is varied. Still, final core masses in the *mixing* and *rainout* cases do not vary much from 0.4 and $0.6 M_{\oplus}$, respectively. This can be explained by noting that increasing the accretion rate of pebbles causes two competing effects on pebble impacts and absorption rates. Firstly, higher accretion rates lead to increased luminosity and thus to higher temperatures, causing more ablation. At the same time however, these higher temperatures reduce gas densities and thus inhibit gas drag. The result is that pebbles fully evaporate at a similar core mass, but at a significantly lower envelope mass (not shown in table). Similarly for absorption rates, higher accretion rates mean that the temperature at which silicates vaporize, starts further from the core, but at a lower density. The same effects also influence the final core mass as a function of position, where a planet’s envelope closer to the central star

is hotter and less dense. In our model, final core masses tend to decrease as the planet’s location moves closer to the star.

It is found that the core formation process is most sensitive to changes in the mean molecular weight of the high-Z constituent SiO_2 . This value determines the density scaling of the high-Z layer near the core and therefore has a great influence on how much vapor this layer can contain. While it is a well known constant, it is possible that impactors constitute of different materials or that SiO_2 can dissociate into other chemical compounds with lower mean molecular weight. Our simulations show that the final core mass of the *rainout* case increases to $1.49 M_{\oplus}$ when we reduce the mean molecular weight of SiO_2 all the way to 10. We have also included a variation of the adiabatic index because this value is less well known. It is found not to have a large impact on the resultant core masses. As a comparison, we have performed an additional simulation without considering any enrichment effect, where all ablated material falls to the core. In this case we found that the core grew to $9.1 M_{\oplus}$, at which point gas accretion became dynamically unstable and our simulation was stopped. This value for the critical core mass is consistent with previous calculations that assumed low (grain-free) opacities (e.g. Mizuno 1980; Hori & Ikoma 2010).

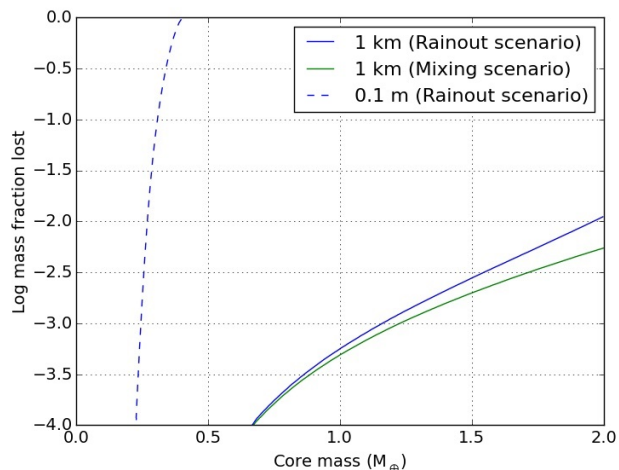


Fig. 5. The ablation curves for 1 km planetesimals (solids curves) and 0.1 m pebbles (dashed curve) impacting a growing proto-planet. The green line indicates the *mixing* case and the blue line represents the *rainout* scenario. The dashed 0.1 m curve is almost identical for both enrichment assumptions (*rainout* plotted). Ablation rates are limited to approximately 1 % up to a core mass of $2 M_{\oplus}$.

Finally, Table 2 shows that final core masses do not change when we switch from an ideal gas to a more sophisticated equation of state for a mixture of hydrogen, helium and SiO_2 . We find that the ideal gas with high mean molecular weight yields similar P-T-rho behavior in comparison to the tested model of Vazan et al. (2013). The reason is that, while the temperatures and densities near the core can exceed those required for non-ideal gas effects such as hydrogen dissociation, this hot inner region consists mainly of silicates (see Fig. 4). Hydrogen and helium are the envelope’s main constituents in the region outside this layer where temperatures are lower.

4. Comparison with classical core accretion

In order to make our results comparable to calculations of classical core accretion, we repeat the previous core growth simulation with 1 km planetesimals instead of pebbles. We consider 1 km planetesimals for two reasons. Firstly, they are relatively sensitive to ablation compared to more massive planetesimals. If ablation effects for these planetesimals are too small to become of great importance, this must also be true for larger impactors. Secondly, when impactors are sufficiently massive, they become dynamically stable due to their self-gravity. For rocky impactors this can happen when the radius exceeds about 70 km (Podolak et al. 1988). We use a typical planetesimal accretion rate of $10^{-6} M_{\oplus} \text{ yr}^{-1}$ (e.g. Pollack et al. 1996). For our purposes, the most important contrast between pebble and classical core accretion is the difference in mass deposition. Larger impactors slow down less quickly in the hot inner region and have a lower area to mass ratio. Figure 5 shows the mass fraction that 1 km planetesimals have lost upon core impact. Ablation rates remain limited to one percent even up to a core growth of $2 M_{\oplus}$, which is consistent with previous calculations, in which planetesimals are assumed to reach the core intact.

Instead of ablation, the breakup of planetesimals during impact is typically expected to be the main cause of their mass deposition (Podolak et al. 1988). If breakup is expected to typically occur far away from the core ($r_{\text{breakup}} \gg R_{\text{core}}$), their post-breakup material can slow down and enrich the envelope. In this

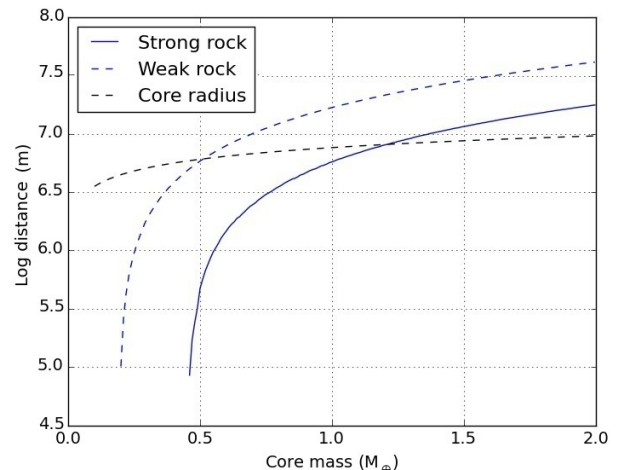


Fig. 6. The distance to the core at breakup for 1 km planetesimals impacting a growing proto-planet. The solid blue curve belongs to strong rock and the dashed blue curve to weak rock. The curves are almost identical for both enrichment assumptions (*rainout* plotted). The black dashed curve represents the core radius.

case, core growth might look similar to pebble accretion. But if breakup is not expected to occur until the planet is more massive, or it happens close to the core ($r_{\text{breakup}} \ll R_{\text{core}}$), it is reasonable to assume that any post-breakup material reaches the core. In this case the planet does not become similarly enriched and core growth is much extended.

To calculate breakup points, we checked where in the envelope dynamical pressures first exceeded the compressive strength of the planetesimal. For this we used typical rock strengths of 1 MPa and 10 MPa for weak and strong rock respectively (e.g. Petrovic 2001; Popova et al. 2011; D’Angelo & Podolak 2015). The breakup distances are plotted in Fig. 6 along with the core radius.

Strong planetesimals are found to be resilient to breakup before the core mass exceeds $0.5 M_{\oplus}$. Thereafter, the breakup point remains relatively close to the core ($r_{\text{breakup}} < 2R_{\text{core}}$) up to at least $2 M_{\oplus}$. In the weak limit, breakup can happen for core sizes as small as $0.2 M_{\oplus}$. The point of breakup exceeds the core radius at $0.5 M_{\oplus}$ and becomes approximately $4 \times r_{\text{core}}$ at $2 M_{\oplus}$. This means that we cannot fully exclude the possibility for planetesimal breakup material to enrich the atmosphere in the early stages of formation, however this can only occur if the planetesimals are relatively weak.

If we ignore the possible effects of breakup, we can simulate the planet’s growth using exactly the same code as before. We then find that the envelope becomes dynamically unstable due to the accretion of disk gas when the core has grown to several M_{\oplus} . The final core masses we found were $2.8 M_{\oplus}$ for the *rainout* case and 5.0 for *mixing*.

5. Discussion and conclusions

Planet formation by pebble accretion is an alternative to the classical, planetesimal-driven core accretion scenario. Their two main differences are a higher expected solids accretion rate and more rapid ablation in the case of pebbles. In this work, we focus on the second difference and analyzed its effect on core growth. To accomplish this, we have simulated the early formation of planets for both the pebble and classical core accretion

scenario's, using a code consisting of two components: both an impact and a planet evolution model. We find that the rapid ablation of pebbles changes the process of core growth. It means that pebbles can be prevented from directly reaching the core of even a small growing planet. Instead, their ablated material can either rain out to the core or be absorbed by the envelope as vapor. We have incorporated these enrichment effects from the moment that pebbles first start ablating by modifying the mean molecular weight and gas characteristics locally where high-Z material is present in vapor form.

We find that impacting SiO_2 pebbles can already fully ablate upon impact with planets of mass less than $0.5 M_{\oplus}$. The amount of high-Z material that can stay in vapor form is heavily temperature dependent. This means that only the envelope's inner region is able to retain it, leading to the formation of a high-Z layer surrounding the core, where temperatures are highest. At first this region is small and unable to contain large amounts of vapor. Most ablated material then rains out to the core. Core growth slows down as the high-Z region expands outwards over time, increasing ablation for subsequent impactors and preventing their mass from reaching the core by absorbing it as vapor. This process limits direct core growth by pebbles to about $0.6 M_{\oplus}$. Our findings are relatively insensitive to the planet's position in the accretion disk, pebble sizes up to 1m, or the solids accretion rate. They depend most sensitively on the mean molecular weight of the high-Z material (SiO_2) and the adopted expression for the vapor pressure, Eq. (30). The mean molecular weight determines the steepness of the temperature and density curves in the inner region while vapor pressure determines its size and influences pebble ablation profiles.

By repeating our simulations with 1 km impacting planetesimals, we have shown that enrichment due to ablation is minimal if the impactors are sufficiently massive. Impacting planetesimals are resilient to ablation up to planet masses of several M_{\oplus} . Mass deposition via breakup is only expected to occur close to the core-envelope boundary, which makes it likely that post-breakup material can reach the core. The ability of planetesimals to reach the core-envelope boundary and the resultant lack of enrichment during the first stage of core growth allows massive cores to form more easily in classical core accretion.

In our model, we only use impactors with a uniform rocky (SiO_2) composition. In reality it is expected that outside the disk iceline, impactors constitute of a mix of rocky and icy pebbles. We chose not to include the ices due to their lower evaporation temperature, and our focus on core growth. Pebbles made of H_2O -ice will evaporate further away from the core than rocky ones, after which they can be absorbed by the atmosphere as vapor. Subsequently, the H_2O vapor can either remain in the envelope where it increases the mean molecular weight and speeds up the envelope collapse (Venturini et al. 2015), or recycle outwards into the disk (Ormel et al. 2015; Cimerman et al. 2017; Lambrechts & Lega 2017). In both cases, H_2O does not contribute to any further core growth. Rocky materials require higher temperatures to vaporize and can therefore continue to grow the core. An implication of this finding is that only rocky cores can be formed by pebble accretion, whereas icy cores must thus be formed by impacts of larger, planetesimal-sized impactors.

Recently, Alibert (2017) has suggested that, if recycling operates vigorously and the envelope becomes fully mixed, any high-Z material present in the envelope will recycle back to the disk. In that case, direct core growth is the only growth mechanism in pebble accretion, core masses would be limited to $0.6 M_{\oplus}$, and enrichment of the envelope would be very low. However, there are two arguments against his hypothesis of efficient

mixing. First, recent hydrodynamical simulations involving radiation transport have shown that hydrodynamical recycling operates less efficiently in the inner-most regions where we expect the high-Z vapors to be concentrated (Cimerman et al. 2017; Lambrechts & Lega 2017). Second, the high-Z vapor will congeal when it is transported to cooler regions. These grains will subsequently rain out to the core, unless they can be very efficiently mixed with the outer envelope, i.e. by regular (eddy) convection. Conceivably, luminosity sources from radioactive heating or core cooling (Vazan et al. 2017 in prep.) could provide the required luminosity.

However, in order to mix grains to the outer envelope, the (convective) mixing times must be shorter than the settling timescale ($\tau_{\text{mix}} < \tau_{\text{settle}}$). Besides this, mixing is only effective if the planet contains a large convective region. In our work, we find that the convective region is comparatively small and shielded by a large isothermal, radiative zone (see Fig. 4). Therefore, we argue that the planet is likely to retain its high-Z vapor against recycling.

Under these conditions the formation of a high-Z layer, situated between the core and the H/He envelope, is an integral part of planet formation by pebble accretion. It can be considered as a dilute extension of the core, with densities approaching the core density and a metal-poor surrounding envelope. This is similar to envelope structures found by other works that considered a temperature-localized high-Z region in giant planets (Helled & Stevenson 2017; Lozovsky et al. 2017). Upon further accretion of pebbles, the high-Z region will keep expanding outwards, increasing in mass along with the H/He-region. Similar to the classical scenario, this will end when hydrostatic balance can no longer be maintained. However, accretion of pebbles may already terminate before this point. In that case the proto-planet will evolve through Kelvin-Helmholtz cooling of the envelope. Because of the cooling, we then expect the high-Z layer to rain out to the core. This is the way how we envision core growth to super-Earth and mini-Neptune sizes by pebble accretion.

To summarize, we find that pebble accretion can only directly form rocky cores up to $0.6 M_{\oplus}$, and is unable to form icy cores. This contrasts with classical core accretion, which can directly produce much more massive cores with various compositions. The reason for limited direct core growth in pebble accretion is that pebbles ablate more rapidly upon impact. Their subsequent absorption by the surrounding gas prevents their mass from reaching the core when the envelope becomes sufficiently hot and massive. Core growth after this point may proceed through new indirect processes if the planet is able to retain its high-Z material. The expected localization of SiO_2 vapors near the core can prevent it from being recycled into the disk and facilitate future core growth when the planet cools down. Further research is required to explore these later stages of core growth, and we will study it in a future work.

Acknowledgements

C.W.O. is supported by The Netherlands Organization for Scientific Research (NWO; VIDI project 639.042.422)

References

- Adolfsson, L. G., Gustafson, B. Å. S., & Murray, C. D. 1996, *Icarus*, 119, 144
- Alibert, Y. 2017, ArXiv e-prints, 1705.06008
- Alibert, Y., Mordasini, C., Benz, W., & Winisdoerffer, C. 2005, *A&A*, 434, 343
- Bell, K. R. & Lin, D. N. C. 1994, *The astrophysical journal*, 427, 987
- Benz, W., Mordasini, C., Alibert, Y., & Naef, D. 2006, in *Tenth Anniversary of 51 Peg-b: Status of and prospects for hot Jupiter studies*, ed. L. Arnold, F. Bouchy, & C. Moutou, 24–34

- Bitsch, B., Lambrechts, M., & Johansen, A. 2015, *A&A*, 582, A112
- Brown, P. P. & Lawler, D. F. 2003, *Journal of Environmental Engineering*, 129, 222
- Chambers, J. E. 2014, *Icarus*, 233, 83
- Chase, M. 1998, *J. Phys. Chem. Ref. Data*, 1952
- Cimerman, N. P., Kuiper, R., & Ormel, C. W. 2017, ArXiv e-prints
- D'Angelo, G. & Podolak, M. 2015, *ApJ*, 806, 203
- Dean, J. A. 1985, 509
- Hayashi, C. 1981, *Progress of Theoretical Physics Supplement*, 70, 35
- Helled, R. & Stevenson, D. 2017, *ApJ*, 840, L4
- Hori, Y. & Ikoma, M. 2010, *ApJ*, 714, 1343
- Hubickyj, O., Bodenheimer, P., & Lissauer, J. J. 2005, *Icarus*, 179, 415
- Iaroslavitz, E. & Podolak, M. 2007, *Icarus*, 187, 600
- Ida, S., Guillot, T., & Morbidelli, A. 2016, *A&A*, 591, A72
- Kobayashi, H., Tanaka, H., Krivov, A. V., & Inaba, S. 2010, *Icarus*, 209, 836
- Lambrechts, M. & Johansen, A. 2012, *A&A*, 544, A32
- Lambrechts, M., Johansen, A., & Morbidelli, A. 2014, *A&A*, 572, A35
- Lambrechts, M. & Lega, E. 2017, ArXiv e-prints
- Levison, H. F., Thommes, E., & Duncan, M. J. 2010, *AJ*, 139, 1297
- Love, S. G. & Brownlee, D. E. 1991, *Icarus*, 89, 26
- Lozovsky, M., Helled, R., Rosenberg, E. D., & Bodenheimer, P. 2017, *ApJ*, 836, 227
- McAuliffe, J. P. & Christou, A. A. 2006, *Icarus*, 180, 8
- Melosh, H. J. & Goldin, T. J. 2008, in *Lunar and Planetary Science Conference*, Vol. 39, *Lunar and Planetary Science Conference*, 2457
- Michaelides, E. E. 2006, 107
- Mills, A. F. 1999, *Basic heat and mass transfer (Pearson College Div)*, 371–372
- Mizuno, H. 1980, *Progress of Theoretical Physics*, 64, 544
- Morbidelli, A. & Nesvorný, D. 2012, *A&A*, 546, A18
- Mordasini, C. 2014, *Astronomy & Astrophysics*, 572, A118
- Mordasini, C., Alibert, Y., Klahr, H., & Henning, T. 2012, *A&A*, 547, A111
- Movshovitz, N., Bodenheimer, P., Podolak, M., & Lissauer, J. J. 2010, *Icarus*, 209, 616
- Ormel, C. W. 2014, *ApJ*, 789, L18
- Ormel, C. W. 2017, in *Formation, Evolution, and Dynamics of Young Solar Systems*, ed. Pessah, M. & Gressel, O., *Proceedings of the Sant Cugat Forum on Astrophysics (Springer)*
- Ormel, C. W. & Klahr, H. H. 2010, *A&A*, 520, A43
- Ormel, C. W., Shi, J.-M., & Kuiper, R. 2015, *MNRAS*, 447, 3512
- Petrovic, J. 2001, *Journal of Materials Science*, 36, 1579
- Pinhas, A., Madhusudhan, N., & Clarke, C. 2016, *MNRAS*, 463, 4516
- Piso, A.-M. A. & Youdin, A. N. 2014, *ApJ*, 786, 21
- Podolak, M., Pollack, J. B., & Reynolds, R. T. 1988, *Icarus*, 73, 163
- Pollack, J. B., Hubickyj, O., Bodenheimer, P., et al. 1996, *Icarus*, 124, 62
- Popova, O., Borovička, J., Hartmann, W. K., et al. 2011, *Meteoritics and Planetary Science*, 46, 1525
- Powell, R., Ho, C. Y., & Liley, P. E. 1966
- Stull, D. R. 1947, *Industrial & Engineering Chemistry*, 39, 517
- Vazan, A., Kovetz, A., Podolak, M., & Helled, R. 2013, *MNRAS*, 434, 3283
- Venturini, J., Alibert, Y., & Benz, W. 2016, *A&A*, 596, A90
- Venturini, J., Alibert, Y., Benz, W., & Ikoma, M. 2015, *A&A*, 576, A114
- Weidenschilling, S. J. 1977, *Ap&SS*, 51, 153
- Whipple, F. L. 1972, in *From Plasma to Planet*, ed. A. Elvius, 211